Original Article

Proton exchange rate of chemical exchange saturation transfer MRI constructed from direct saturation-removed omega plots to improve the assessment of patients with ischemic stroke

Yiran Zhou[1], Zhenxiong Wang[2], Mehran Shaghaghi[3], Guiling Zhang[1], Hongquan Zhu[1], Di Wu[1], Jun Lu[1], Su Yan[1], Shun Zhang[1], Li Li[1], Jia Li[1], Kejia Cai[3], Wenzhen Zhu[1]

[1]Department of Radiology, Tongji Hospital, Tongji Medical College, Huazhong University of Science and Technology, Wuhan, China; [2]Department of Radiology, Guangzhou First People's Hospital, School of Medicine, South China University of Technology, Guangzhou, China; [3]Department of Radiology, University of Illinois Hospital and Health Sciences System, Chicago, IL, USA

Contributions: (I) Conception and design: Y Zhou, Z Wang, M Shaghaghi, L Li, K Cai, W Zhu; (II) Administrative support: K Cai, W Zhu; (III) Provision of study materials or patients: K Cai, W Zhu; (IV) Collection and assembly of data: Y Zhou, M Shaghaghi, Z Wang, G Zhang, H Zhu, D Wu, J Lu, S Yan, J Li; (V) Data analysis and interpretation: Y Zhou, Z Wang, M Shaghaghi, G Zhang, S Zhang; (VI) Manuscript writing: All authors; (VII) Final approval of manuscript: All authors.

Correspondence to: Wenzhen Zhu, MD, PhD. Department of Radiology, Tongji Hospital, Tongji Medical College, Huazhong University of Science and Technology, 1095 Jiefang Avenue, Wuhan 430030, China. Email: zhuwenzhen8612@163.com; Kejia Cai, PhD. Department of Radiology, University of Illinois Hospital and Health Science System, 1740 W Taylor Street, Chicago, IL 60612, USA. Email: kcai@uic.edu.

Background: Proton exchange rate (k_{ex}) magnetic resonance imaging (MRI) has recently been developed, with preliminary results demonstrating its potential for evaluating reactive oxygen species. This prospective cohort study investigated the k_{ex} in different stroke stages and its correlation with stroke severity and prognosis.

Methods: In all, 96 ischemic stroke patients were included in the study. Patients were divided into 3 groups based on stroke phase (acute, subacute, and chronic). A spin echo-echo planar imaging sequence with presaturation powers of 1.5, 2.5, and 3.5 μT was implemented to obtain Z-spectra, and k_{ex} maps were constructed from direct saturation-removed omega plots. Relative k_{ex} (rk_{ex}) and the relative apparent diffusion coefficient (rADC) were calculated as the ratio of k_{ex} or ADC in the infarcts to values in contralateral tissue, respectively. Correlations between both k_{ex} and rk_{ex} and National Institute of Health Stroke Scale (NIHSS) scores were evaluated. Receiver operating characteristic (ROC) analysis was used to evaluate the performance of k_{ex}, rk_{ex}, rADC, and lesion volume for predicting acute stroke outcome.

Results: The k_{ex} was significantly higher in ischemic lesions than in contralateral tissue at all stages. In addition, the k_{ex} of acute lesions was higher than that of subacute and chronic lesions [mean (± SD) 935.1±81.5 *vs.* 881.4±55.7 and 866.9±76.7 s^{-1}, respectively; P<0.05 and P<0.01, respectively]. The difference in k_{ex} between subacute and chronic lesions was not significant. In acute stroke, there was a limited correlation between a lesion's k_{ex} and NIHSS score (R^2=0.16; P=0.01) and between rk_{ex} and NIHSS score (R^2=0.28; P=0.001). Acute stroke patients with poor prognosis had significantly higher lesion k_{ex} and rk_{ex} than did those with good prognosis (k_{ex}: 991.1±78.2 *vs.* 893.1±55.1 s^{-1}, P<0.001; rk_{ex}: 1.28±0.09 *vs.* 1.15±0.06, P<0.001). In ROC analyses, k_{ex} and rk_{ex} showed favorable predictive performance for acute stroke outcome, with areas under the curve (AUC) of 0.837 and 0.880, respectively, which were slightly but not significantly higher than the AUCs for lesion volume (0.730) and rADC (0.673).

Conclusions: This study indicates that k_{ex} MRI is promising for the diagnosis and management of ischemic stroke because it can reflect the oxidative stress of lesions and predict prognosis.

Keywords: Chemical exchange saturation transfer; ischemic stroke; prognosis; proton exchange rate

Submitted Jan 15, 2022. Accepted for publication Jul 13, 2022.
doi: 10.21037/qims-22-78
View this article at: https://dx.doi.org/10.21037/qims-22-78

Introduction

As a common disease, stroke affects one-quarter of people during their lifetime and is the second leading cause of death and the third leading cause of disability among adults worldwide (1). Magnetic resonance imaging (MRI) has played a key role in the assessment of stroke severity and recovery (2-4). The development of imaging technology has enabled the detection of hemodynamics and various metabolic biomarkers in ischemic tissues, which is instrumental in further understanding the pathophysiological mechanisms of ischemic stroke and thus improving the therapeutic approach (5-7).

Chemical exchange saturation transfer (CEST) MRI is an emerging endogenous metabolic technique in which the contrast is produced by the transfer of selectively saturated protons from endogenous metabolites to bulk water (8). Various studies have used CEST in the metabolic assessment of ischemic stroke (3,9,10). Proton exchange is a fundamental biophysical process that is critical to generating CEST MRI contrasts. Based on direct saturation-removed omega plots, *in vivo* imaging of the proton exchange rate (k_{ex}) has been recently developed (11).

The k_{ex} MRI has been used in phantoms and healthy brains (11) as well as in characterizing multiple sclerosis lesions (12). A recent study investigating the performance of k_{ex} in subacute and chronic stroke patients found that k_{ex} maps, which showed differences compared with the contrast of diffusion-weighted imaging (DWI), could favorably differentiate ischemic stroke lesions from contralateral healthy tissue (13). Nevertheless, the small sample size and lack of acute stroke patients in that study could not fully demonstrate the clinical application of k_{ex} maps. The previous study (13) has reported the enhanced k_{ex} in ischemic lesions to be due to increases in reactive oxygen species (ROS), which have been shown to play a crucial role in the pathogenesis of ischemic brain injury (14). The dynamic changes in k_{ex} in ischemic tissue deserve further investigation because they can help elucidate the detailed environmental evolution of the infarcted area and improve our understanding of the pathophysiology of stroke. In addition, the correlation between k_{ex} and both stroke severity and prognosis has not yet been investigated. Prompt and exact predictions of outcomes in acute stroke patients would aid in clinical decision making, facilitate individualized treatments, and improve prognosis (15).

The aims of this study were to evaluate changes in k_{ex} in ischemic lesions at different stages of stroke and to explore the correlations between k_{ex} and stroke severity. Furthermore, we assessed the predictive performance of k_{ex} for acute stroke prognosis by comparing it with traditional MRI parameters, including infarct volume and the apparent diffusion coefficient (ADC), which have demonstrated predictive efficacy for stroke outcome (16,17). We present the following article in accordance with the STROBE reporting checklist (available at https://qims.amegroups.com/article/view/10.21037/qims-22-78/rc).

Methods

This study was conducted in accordance with the Declaration of Helsinki (as revised in 2013). This specific type of observational study was approved by the Institutional Review Board of Tongji Hospital Affiliated to Tongji Medical College of Huazhong University of Science and Technology. All participants were informed of the detailed experimental procedures and signed informed consent forms.

Sample size estimation

The sample size was estimated using Power Analysis and Sample Size software (NCSS, LLC, Kaysville, Utah 84037, USA) and based on a previous study (13). The following settings were used in calculating sample size: power =0.9; alpha =0.05; number of groups =3; allocation ratio =1.0; group means =940, 900, and 875; and SD =70. Based upon this, the least number of measurements required was determined to be 30 participants per group.

Study population

In all, 117 ischemic stroke patients who presented to Wuhan Tongji Hospital between December 2018 and November 2021 were enrolled in the study. To be eligible for inclusion in the study, patients had to have (I) been diagnosed with unilateral ischemic stroke, (II) no previous

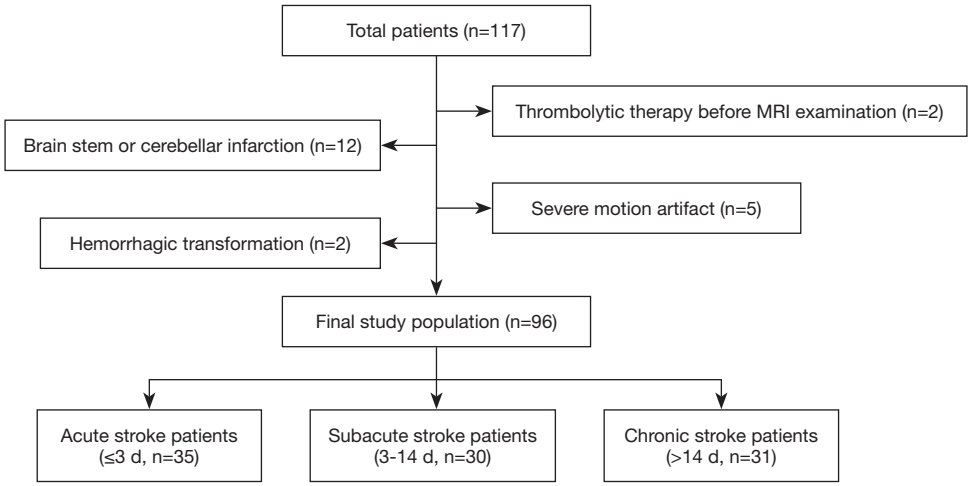

Figure 1 Flow diagram of patient selection and grouping. MRI, magnetic resonance imaging.

stroke history, (III) a known time of symptom onset, (IV) no other nervous system disorders or systemic diseases, and (V) undergone DWI and CEST MRI (Z-spectral imaging scans). Twenty-one patients were excluded from the present study due to hemorrhagic transformation (n=2), brain stem or cerebellar infarction (n=12), thrombolytic therapy before MRI examination (n=2), or severe motion artifact (n=5).

The 96 patients recruited to this study were divided into following 3 groups based on the onset-to-MRI time (18): acute phase (onset-to-MRI time ≤3 days; n=35), subacute phase (3–14 days; n=30), and chronic phase (>14 days; n=31). Stroke severity was evaluated in patients before MRI examinations by a neurologist (ZS, 7 years' experience) using the National Institute of Health Stroke Scale (NIHSS) score. The prognosis of acute stroke patients was assessed using the modified Rankin Scale (mRS) score at 3 months after discharge through a structured telephone interview performed by another neurologist (ZGL, 5 years' experience) who was blinded to all clinical and image data. No patients were lost to follow-up. Prognosis was dichotomized into good (mRS score ≤2) and poor (mRS score >2). Details of patient selection and grouping are shown in *Figure 1*.

MRI acquisition

All MRI scans were performed using a 3.0-T MRI system (Discovery MR750; GE Healthcare, Waukesha, WI, USA) with a 32-channel head coil. DWI was used to localize the infarction. Single-slice CEST Z-spectral data were acquired on an axial slice where the largest infarction was located with reference to DWI, and the acquisition method for the CEST MRI was a spin echo-echo planar imaging sequence. The parameters for DWI were as follows: repetition time (TR) =3,000 ms, echo time (TE) =65.7 ms, field of view (FOV) =240×240 mm, matrix size =160×160, in-plane resolution =1.5×1.5 mm, slice thickness =5 mm, b=0, and 1,000 s/mm^2. The parameters for Z-spectral data acquisition were as follows: TR =6,114 ms; TE =22.6 ms; FOV =240×240 mm; matrix size =160×160; in-plane resolution =1.5×1.5 mm; slice thickness =5 mm; number of excitation =1; amplitude of saturation radiofrequency (RF) =1.5, 2.5, and 3.5 μT; duration of saturation RF =1,500 ms; and number of saturation RF =4. Each Z-spectrum included 33 images obtained at the following saturation offsets: +39.1, +15.6, ±6, ±5, ±4.5, ±4, ±3.75, ±3.5, ±3.25, ±3, ±2.5, ±2, ±1.5, ±1, ±0.75, ±0.5, ±0.25, and 0 ppm. The scanning time for each of the three Z-spectral data was 3 min and 22 s.

Data analysis

Previously developed programs in MATLAB (MathWorks, Natick, MA, USA) were used for the processing and analysis of raw data (13). Initially, the motion artifacts of Z-spectral images were rectified by the intensity-based image registration routine "imregister" in MATLAB, using the "translation" transform type with 2 degrees of freedom. Based on the B_0 map generated from the Z-spectrum collected at the lowest saturation RF power (1.5 μT), all Z-spectral data underwent B0 correction. The Z-spectra were inverted to be $100\times(1–M_z/M_0)$, with M_0 (the Z-spectrum signal at 39.1 ppm) being used as

the reference for M_z (the Z-spectrum signal at +3.5 ppm, the conventional amide proton resonance). The spectra were then fitted to a linear combination of 2 Lorentzian functions corresponding to the bulk water direct saturation and all the residual effects [magnetization transfer (MT) from semisolid components, CEST, and nuclear overhauser enhancement (NOE)]. Next, the bulk water peak was subtracted from the original Z-spectra, and the residual signals were used to establish the omega plot. As the various exchange mechanisms (MT, NOE, CEST) would contribute to the tissue k_{ex}, the omega plot was extended and generalized in order to include all proton-exchange sources, as has been done previously (11,13). As a result, the linear relationship between $\frac{M_z}{M_0 - M_z}$ (the inverse of the Z-spectral signal intensities) and $\frac{1}{\omega_1^2}$ (the inverse of the square of the saturation RF powers) would indicate that the *x*-axis intercept of the omega plot can provide a weighted average readout of the intricate tissue k_{ex} contributed to by the various exchange mechanisms, including CEST, MT, and NOE (13).

Considering that the ischemic area shown on the k_{ex} maps typically differs from that on ADC maps (13), to ensure the accuracy of k_{ex} calculations in lesions, the regions of interest (ROIs) of stroke lesions were drawn on the k_{ex} maps by an experienced neuroradiologist (WZX, 6 years' experience) and double-checked by another neuroradiologist (LL, 10 years' experience). Both neuroradiologists were blinded to the patient information. The k_{ex} of the ROI was considered the mean value of all pixels. To calculate the relative k_{ex} (rk_{ex}), the k_{ex} of the infarcted ROIs was divided by the k_{ex} of contralateral (normal) tissue.

For the 35 acute stroke survivors, DWI data were imported into the GE ADW 4.6 workstation to generate ADC maps. To calculate infarct volume, the hypointense ischemic lesions were manually drawn on the ADC maps using ITK-SNAP software (version 3.8.0, the University of Pennsylvania and the University of Utah, USA) by a neuroradiologist (WD, 5 years' experience) who was blinded to the clinical data. The relative ADC (rADC) was calculated for the slice corresponding to the k_{ex} map as the ratio of the signal intensity of the infarct area to that of contralateral (normal) tissue.

Statistical analysis

All statistical analyses were conducted using IBM SPSS statistics (version 26; IBM Corp., Armonk, NY, USA) and R (version 3.6.3; R Foundation for Statistical Computing, Vienna, Austria). One-way analysis of variance (ANOVA) and the chi-squared test were used to compare demographics between groups. The k_{ex}, rk_{ex}, and rADC datasets used in the analysis were all normally distributed (Kolmogorov-Smirnov test) and had equal variance (Levene test). The significance of differences in k_{ex} between different stroke phases and different ROIs was evaluated using one-way ANOVA with a post hoc Bonferroni test and 2-tailed paired *t* tests, respectively. Coefficients of determination (R^2) were used to evaluate correlations between both k_{ex} and rk_{ex} and the NIHSS score. Independent-samples *t* test, the Mann-Whitney U test, and the chi-squared test were used to compare age, sex, k_{ex}, rk_{ex}, rADC, and infarct volume between patients with different prognoses. The receiver operating characteristic (ROC) curve was used to evaluate the predictive performance of these parameters for prognosis. The DeLong test was used to compare different areas under the curve (AUC). Unless indicated otherwise, data are presented as the mean ± SD. A 2-sided P value <0.05 was considered statistically significant.

Results

Figure 2A shows Z-spectra data from a representative stroke lesion at different saturation RF powers. *Figure 2B* shows the fitted Z-spectrum for the bulk water direct saturation and the residual signal. Omega plots for the quantification of k_{ex} in the stroke lesion or the contralateral tissue are shown in *Figure 2C*. The 95% CIs of the slope and x-axis intercept in the linear fitting of the omega plots are presented in Table S1.

The clinical information for the 96 patients, along with k_{ex} and rk_{ex}, is presented in *Table 1*. Representative DWI, ADC maps, and k_{ex} maps for each of the 3 ischemic stroke phases are shown in *Figure 3*. The ischemic stroke lesions in each of the 3 phases are all distinctly delineated, with markedly elevated intensity on k_{ex} maps.

As shown in *Figure 4*, the k_{ex} of the ischemic lesions was significantly higher than that of the contralateral tissue in all stroke phases (acute phase: 935.1±81.5 *vs.* 777.3±45.1 s^{-1}, P<0.001; subacute phase: 881.4±55.7 *vs.* 762.2±36.6 s^{-1}, P<0.001; chronic phase: 866.9±76.7 *vs.* 756.3±36.7 s^{-1}, P<0.001). The percentage increase in k_{ex} relative to the contralateral tissue in the acute, subacute, and chronic phases was 20.3%, 15.6%, and 14.6%, respectively. In addition, the k_{ex} of the ischemic lesions was higher in the

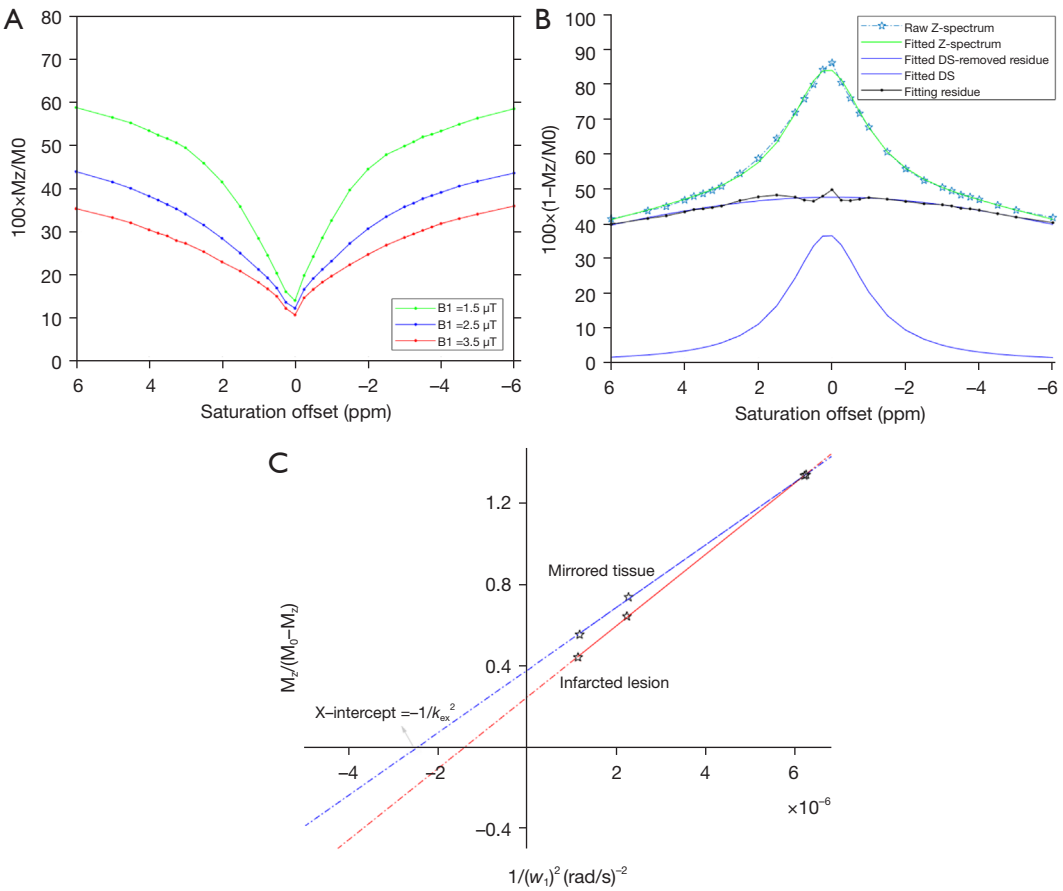

Figure 2 Process showing the quantification of the k_{ex} in the brain. (A) Typical Z-spectra from an ischemic lesion for 3 different B_1: 1.5, 2.5, and 3.5 μT. (B) Water DS was removed by Lorentzian fitting at a B_1 of 1.5 μT. The omega plot was established on the basis of residual signals after the subtraction of DS. (C) Representative DS-removed omega plots of an ischemic lesion (red line) and contralateral tissue (blue line). The *x*-axis intercept of this plot provides a readout of k_{ex}. k_{ex}, proton exchange rate; B_1, saturation power; DS, direct saturation.

acute phase than in both the subacute and chronic phases, whereas there was no significant difference in k_{ex} between the subacute and chronic lesions.

Although k_{ex}, rk_{ex}, and the NIHSS score all showed a downward trend from the acute to the chronic phase, the correlation between both k_{ex} and rk_{ex} and the NIHSS score was limited to being significant only for acute stroke lesions (k_{ex}: R^2=0.16, P=0.016; rk_{ex}: R^2=0.28, P=0.001).

The rADC, infarct volume, k_{ex}, and rk_{ex} of acute stroke lesions differed significantly between patients with different prognoses (*Table 2*). In addition, ROC curve analysis demonstrated that k_{ex} and rk_{ex} of the ischemic lesion had favorable predictive efficacy for the prognosis of acute stroke patients, with AUCs of 0.837 and 0.880, respectively (*Figure 5*). The AUCs for k_{ex} and rk_{ex} were higher than those for infarct volume and rADC; however, the DeLong test indicated that there were no significant differences in the AUCs of these 4 parameters (P>0.05).

Discussion

In this study, ischemic stroke lesions showed favorable contrast on k_{ex} maps, with a significantly higher k_{ex} than the contralateral tissue regardless of stroke phases. In addition, k_{ex} values were higher for acute ischemic lesions than for lesions in the subacute or chronic phases. There was a positive correlation between both the k_{ex} and rk_{ex} of acute ischemic lesions and the NIHSS score. In addition, we demonstrated that k_{ex} and rk_{ex} could predict the prognosis of acute ischemic stroke patients with favorable efficacy.

Table 1 Population demographics and proton exchange rate of patients in acute, subacute, and chronic ischemic stroke phases

Characteristics	Acute (≤3 days; n=35)	Subacute (3–14 days; n=30)	Chronic (>14 days; n=31)	P value
Age (years)	57.9±10.6	54.4±11.9	53.8±11.8	0.290
Male sex	26 (74.3)	20 (66.7)	19 (61.3)	0.524
Hypertension	24 (68.6)	16 (53.3)	19 (61.3)	0.453
Diabetes	6 (17.1)	7 (23.3)	10 (32.3)	0.355
Hyperlipidemia	5 (14.3)	4 (13.3)	9 (29.0)	0.203
Coronary heart disease	1 (2.9)	2 (6.7)	3 (9.7)	0.517
Current smoker	16 (45.7)	7 (23.3)	10 (32.3)	0.159
Alcohol	16 (45.7)	8 (26.7)	10 (32.3)	0.251
NIHSS score	8 [4–10]	4 [1.8–8]	3 [1–7]	0.001
k_{ex} (s^{-1})	935.1±81.5	881.4±55.7	866.9±76.7	0.001
rk_{ex}	1.20±0.10	1.16±0.07	1.15±0.07	0.01

Unless indicated otherwise, data are given as the mean ± SD, median [interquartile range], or n (%). P values shown are for differences across the 3 groups. Alcohol, excessive alcohol consumption. k_{ex}, proton exchange rate; NIHSS, National Institutes of Health Stroke Scale; rk_{ex}, relative proton exchange rate.

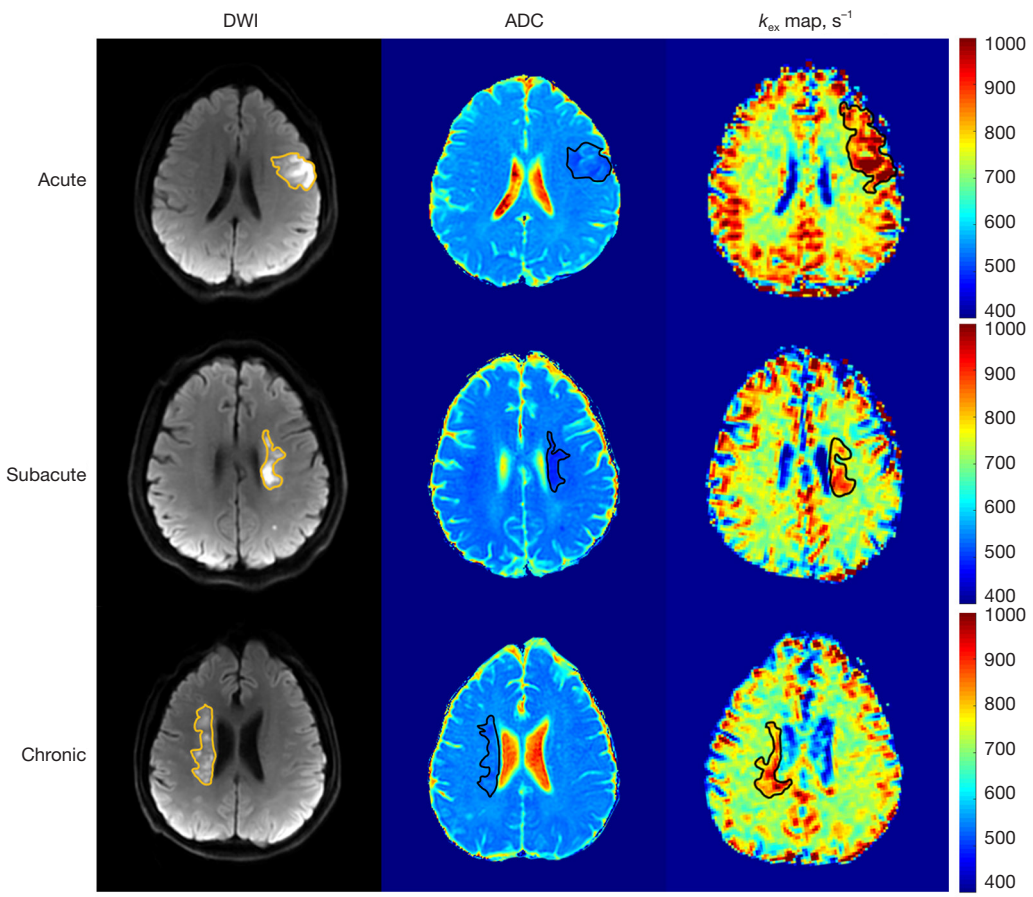

Figure 3 DWI, ADC maps, and k_{ex} maps of representative cases of acute, subacute, and chronic ischemic stroke phases. DWI, diffusion-weighted imaging; ADC, apparent diffusion coefficient; k_{ex}, proton exchange rate.

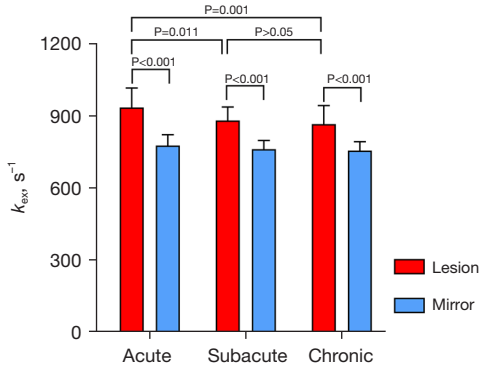

Figure 4 k_{ex} in ischemic lesions and contralateral tissue in the acute, subacute, and chronic ischemic stroke phases. k_{ex}, proton exchange rate.

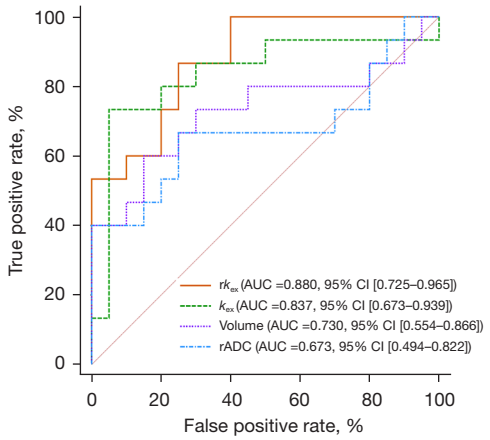

Figure 5 ROC curves of the k_{ex}, rk_{ex}, infarct volume, and rADC for the prediction of prognosis in acute stroke survivors. ROC, receiver operating characteristic; k_{ex}, proton exchange rate; rk_{ex}, relative k_{ex}; rADC, relative apparent diffusion coefficient.

Table 2 Patients' characteristics according to stroke outcome

Characteristics	Good outcome (n=20)	Poor outcome (n=15)	P value
Age (years)	55.2±10.8	61.5±9.7	0.079
Male sex	14 (70.0)	12 (80.0)	0.503
rADC	0.69±0.09	0.61±0.11	0.031
Infarct volume (mL)	2.7 [1.9–8.1]	11.1 [3.0–30.3]	0.021
$k_{ex}(s^{-1})$	893.1±55.1	991.1±78.2	<0.001
rk_{ex}	1.15±0.06	1.28±0.09	<0.001

Unless indicated otherwise, data are given as the mean ± SD, median [interquartile range], or n (%). rADC, relative apparent diffusion coefficient; k_{ex}, proton exchange rate; rk_{ex}, relative proton exchange rate.

A previous study (13) hypothesized that the increased k_{ex} in ischemic lesions may be due to excessive ROS production because the sensitivity and specificity of k_{ex} for ROS has been demonstrated (19). Another study identified 3 distinct phases of ROS generation after cellular ischemia and hypoxia (20). The first increment in ROS occurs during hypoxia and glucose deprivation, coinciding with a period of mitochondrial depolarization. Approximately 25–35 min after ischemia, there is a second increase in ROS due to the activation of xanthine oxidase, whereas the third stage of ROS generation results from improvements in tissue oxygenation levels due to blood flow restoration (20). The acidic environment in stroke lesions increases the H^+ concentrations and thus the rate of conversion of superoxide anion to more reactive ROS, such as hydrogen peroxide (H_2O_2) or the hydroperoxyl radical (HO_2), so as to facilitate oxidation (21). In acute ischemic stroke, lactic acid accumulates in the neurons due to energy depletion, giving rise to acidosis (22). Nevertheless, subacute infarctions are characterized by a shift in pH to alkaline (23). Reduced inflammation over time may be another reason for the decline in k_{ex} of the subacute and chronic infarct lesions relative to the acute lesions, as inflammation is the main cause of extracellular ROS production (24). The findings of the present study are consistent with those of previous studies (20,22-24), as k_{ex} was significantly higher in infarct lesions during the acute rather than the subacute and chronic phases.

However, the interpretation of increased k_{ex} in stroke lesions may be more complicated than simply assuming

that the entire change is due to elevated ROS. It is well known that acidosis in stroke lesions decreases the k_{ex} of metabolites (11). This leads to the observation of more metabolites with a relatively faster exchange of protons on CEST MRI and therefore an overall increase in tissue k_{ex}. This may also be one of the reasons why the k_{ex} of ischemic lesions in the acute phase is higher than that of lesions in the subacute and chronic phases. Nevertheless, it is hard to estimate the contribution of acidosis to tissue k_{ex} compared with that of ROS and other potential factors. Future studies in animal models using invasive measurement of tissue ROS are needed to precisely elucidate the correlation between k_{ex} and ROS.

A positive but limited correlation between both k_{ex} and rk_{ex} and NIHSS scores in acute patients was found in the present study. ROS have significant cellular effects, including lipid peroxidation, protein denaturation, enzyme inactivation, and nucleic acid and DNA damage, ultimately leading to tissue destruction and cell death (25). Neuronal cells are very sensitive and vulnerable to oxidative stress due to low antioxidant enzyme activity, high lipid peroxide concentrations, high oxygen consumption, the absence of energy reserves, and the presence of pro-oxidants such as iron (24). In addition, ROS contribute to disruption of the blood-brain barrier and inflammatory processes (26,27). ROS production has been demonstrated to be a pivotal damaging event leading to neuronal death (28). Because the increment in k_{ex} may be not entirely caused by elevated ROS, only limited correlations were found for k_{ex} and rk_{ex} with NIHSS scores in acute stroke survivors examined in this study.

Extracellular ROS in the acute phase of stroke has been shown to be an indicator of stroke prognosis (29). In the present study, k_{ex} and rk_{ex} had a favorable predictive performance for the prognosis of acute stroke. Because the difference in AUCs between k_{ex} and rk_{ex} and traditional parameters (rADC and infarct volume) was not statistically significant (possibly due to the small sample size) and there was no independent verified dataset in this study, the potential predictive value of k_{ex} maps for acute stroke outcome requires further investigation.

The findings of this study may provide support for the application of antioxidant therapy in ischemic stroke, especially in the acute phase. Although antioxidant treatments in the acute phase have been proposed as a neuroprotective strategy in stroke, most antioxidants have not been successfully implemented in the clinical treatment of stroke (26,30). Studies have demonstrated a high sensitivity and specificity of k_{ex} MRI for ROS both *in vivo* and *in vitro* experiments as well as the potential of k_{ex} MRI to reflect ROS levels in tissues *in vivo* (13,19). Thus, k_{ex} MRI may have potential as a noninvasive tool to monitor the efficacy of antioxidant treatments in real time, thereby facilitating the development of new antioxidant treatments or personalized treatment doses. In addition, k_{ex} MRI could be implemented to further stratify Gd-negative multiple sclerosis lesions based on inflammatory status (12). We believe that k_{ex} MRI will play a growing role in the imaging assessment of various diseases in the future because oxidative stress is associated with the pathogenesis of numerous diseases, including cancer and neurodegenerative diseases (25).

This study has several limitations. First, hyperacute (<6 h) stroke patients were not recruited to the study due to time constraints, and the study did not longitudinally assess the k_{ex} of the same patient at different stroke phases. Longitudinal imaging may be performed in future research to better clarify the progression or recovery of stroke lesions. Second, a scanning time of almost 10 min may not be tolerable for some patients, and thus using only 2 Z-spectra and reducing the number of saturation offsets to considerably shorten the scanning time could enhance clinical application. However, this may affect the precision of k_{ex} determination (11). Third, the ADC value was simply calculated by a 2-point fitting, and it represented a combination of perfusion and diffusion because it was determined using a b value of 0 s/mm^2. The predictive efficacy of ADC may be improved with advanced diffusion models, such as the stretched exponential model (31), intravoxel incoherent motion (32), and fractional-order calculus (33). Fourth, the increments in the vicinity of the water signal were 0.25 ppm in this study, which is relatively coarse because increments of 0.1–0.2 ppm are often used in the water saturation shift referencing method (34). Nevertheless, our method is based on the fitting of the entire Z-spectrum, and we expect the effect due to the 0.25-ppm increment to be negligible. Using 200 ppm as a saturation frequency instead of 39.1 ppm may be a better choice because it is further from water. However, the difference in normalization is similar to all Z-spectra collected at different saturation powers for omega plots, minimizing the effect on the omega plot quantification of tissue k_{ex}. Finally, pathological evidence was absent in this study, but this will be collected in animal models in future studies.

Conclusions

In summary, by on previous studies, we further

demonstrated the feasibility of k_{ex} MRI for ischemic stroke. The k_{ex} was significantly higher for acute stroke lesions than for subacute and chronic lesions. In addition, there was a slight statistical correlation between k_{ex} and stroke severity, indicating its potential for the prediction of prognosis of ischemic stroke patients. With sensitivity to ROS or free radicals, k_{ex} MRI could have considerable potential in the clinical management of stroke and other neurological diseases.

Acknowledgments

Funding: This work was supported by the National Natural Science Foundation of China (Nos. 81730049, 81801666, and 82001782).

Footnote

Reporting Checklist: The authors have completed the STROBE reporting checklist. Available at https://qims.amegroups.com/article/view/10.21037/qims-22-78/rc

Conflicts of Interest: All authors have completed the ICMJE uniform disclosure form (available at https://qims.amegroups.com/article/view/10.21037/qims-22-78/coif). The authors have no other conflicts of interest to declare.

Ethical Statement: The authors are accountable for all aspects of the work in ensuring that questions related to the accuracy or integrity of any part of the work are appropriately investigated and resolved. This study was conducted in accordance with the Declaration of Helsinki (as revised in 2013). The study was approved by the Institutional Review Board of Tongji Hospital affiliated with Tongji Medical College of Huazhong University of Science and Technology, and informed consent was obtained from all participants.

References

1. Campbell BCV, Khatri P. Stroke. Lancet 2020;396:129-42.
2. Tong DC, Yenari MA, Albers GW, O'Brien M, Marks MP, Moseley ME. Correlation of perfusion- and diffusion-weighted MRI with NIHSS score in acute (<6.5 hour) ischemic stroke. Neurology 1998;50:864-70.
3. Yu L, Chen Y, Chen M, Luo X, Jiang S, Zhang Y, Chen H, Gong T, Zhou J, Li C. Amide Proton Transfer MRI Signal as a Surrogate Biomarker of Ischemic Stroke Recovery in Patients With Supportive Treatment. Front Neurol 2019;10:104.
4. Sztriha LK, O'Gorman RL, Modo M, Barker GJ, Williams SC, Kalra L. Monitoring brain repair in stroke using advanced magnetic resonance imaging. Stroke 2012;43:3124-31.
5. Hernández-Pérez M, Puig J, Blasco G, Pérez de la Ossa N, Dorado L, Dávalos A, Munuera J. Dynamic Magnetic Resonance Angiography Provides Collateral Circulation and Hemodynamic Information in Acute Ischemic Stroke. Stroke 2016;47:531-4.
6. Barca C, Foray C, Hermann S, Döring C, Schäfers M, Jacobs AH, Zinnhardt B. Characterization of the inflammatory post-ischemic tissue by full volumetric analysis of a multimodal imaging dataset. Neuroimage 2020;222:117217.
7. Xu Y, Ringgaard S, Mariager CØ, Bertelsen LB, Schroeder M, Qi H, Laustsen C, Stødkilde-Jørgensen H. Hyperpolarized 13C Magnetic Resonance Imaging Can Detect Metabolic Changes Characteristic of Penumbra in Ischemic Stroke. Tomography 2017;3:67-73.
8. van Zijl PC, Yadav NN. Chemical exchange saturation transfer (CEST): what is in a name and what isn't? Magn Reson Med 2011;65:927-48.
9. Jones KM, Pollard AC, Pagel MD. Clinical applications of chemical exchange saturation transfer (CEST) MRI. J Magn Reson Imaging 2018;47:11-27.
10. Foo LS, Harston G, Mehndiratta A, Yap WS, Hum YC, Lai KW, Mohamed Mukari SA, Mohd Zaki F, Tee YK. Clinical translation of amide proton transfer (APT) MRI for ischemic stroke: a systematic review (2003-2020). Quant Imaging Med Surg 2021;11:3797-811.
11. Shaghaghi M, Chen W, Scotti A, Ye H, Zhang Y, Zhu W, Cai K. In vivo quantification of proton exchange rate in healthy human brains with omega plot. Quant Imaging Med Surg 2019;9:1686-96.
12. Ye H, Shaghaghi M, Chen Q, Zhang Y, Lutz SE, Chen W, Cai K. In Vivo Proton Exchange Rate (kex) MRI for the Characterization of Multiple Sclerosis Lesions in Patients. J Magn Reson Imaging 2021;53:408-15.

13. Wang Z, Shaghaghi M, Zhang S, Zhang G, Zhou Y, Wu D, Zhang Z, Zhu W, Cai K. Novel proton exchange rate MRI presents unique contrast in brains of ischemic stroke patients. J Neurosci Methods 2020;346:108926.
14. Nanetti L, Taffi R, Vignini A, Moroni C, Raffaelli F, Bacchetti T, Silvestrini M, Provinciali L, Mazzanti L. Reactive oxygen species plasmatic levels in ischemic stroke. Mol Cell Biochem 2007;303:19-25.
15. Kim TJ, Lee JS, Oh MS, Kim JW, Yoon JS, Lim JS, et al. Predicting Functional Outcome Based on Linked Data After Acute Ischemic Stroke: S-SMART Score. Transl Stroke Res 2020;11:1296-305.
16. Bevers MB, Vaishnav NH, Pham L, Battey TW, Kimberly WT. Hyperglycemia is associated with more severe cytotoxic injury after stroke. J Cereb Blood Flow Metab 2017;37:2577-83.
17. Engelter ST, Provenzale J, Petrella JR, DeLong DM, Alberts MJ. Infarct volume on apparent diffusion coefficient maps correlates with length of stay and outcome after middle cerebral artery stroke. Cerebrovasc Dis 2003;15:188-91.
18. Rehme AK, Eickhoff SB, Wang LE, Fink GR, Grefkes C. Dynamic causal modeling of cortical activity from the acute to the chronic stage after stroke. Neuroimage 2011;55:1147-58.
19. Tain RW, Scotti AM, Cai K. Improving the detection specificity of endogenous MRI for reactive oxygen species (ROS). J Magn Reson Imaging 2019;50:583-91.
20. Abramov AY, Scorziello A, Duchen MR. Three distinct mechanisms generate oxygen free radicals in neurons and contribute to cell death during anoxia and reoxygenation. J Neurosci 2007;27:1129-38.
21. Saeed SA, Shad KF, Saleem T, Javed F, Khan MU. Some new prospects in the understanding of the molecular basis of the pathogenesis of stroke. Exp Brain Res 2007;182:1-10.
22. Xiong ZG, Zhu XM, Chu XP, Minami M, Hey J, Wei WL, MacDonald JF, Wemmie JA, Price MP, Welsh MJ, Simon RP. Neuroprotection in ischemia: blocking calcium-permeable acid-sensing ion channels. Cell 2004;118:687-98.
23. Zöllner JP, Hattingen E, Singer OC, Pilatus U. Changes of pH and energy state in subacute human ischemia assessed by multinuclear magnetic resonance spectroscopy. Stroke 2015;46:441-6.
24. Jelinek M, Jurajda M, Duris K. Oxidative Stress in the Brain: Basic Concepts and Treatment Strategies in Stroke. Antioxidants (Basel) 2021;10:1886.
25. Allen CL, Bayraktutan U. Oxidative stress and its role in the pathogenesis of ischaemic stroke. Int J Stroke 2009;4:461-70.
26. Rodrigo R, Fernández-Gajardo R, Gutiérrez R, Matamala JM, Carrasco R, Miranda-Merchak A, Feuerhake W. Oxidative stress and pathophysiology of ischemic stroke: novel therapeutic opportunities. CNS Neurol Disord Drug Targets 2013;12:698-714.
27. Zhang Y, Wang T, Yang K, Xu J, Ren L, Li W, Liu W. Cerebral Microvascular Endothelial Cell Apoptosis after Ischemia: Role of Enolase-Phosphatase 1 Activation and Aci-Reductone Dioxygenase 1 Translocation. Front Mol Neurosci 2016;9:79.
28. Sanderson TH, Reynolds CA, Kumar R, Przyklenk K, Hüttemann M. Molecular mechanisms of ischemia-reperfusion injury in brain: pivotal role of the mitochondrial membrane potential in reactive oxygen species generation. Mol Neurobiol 2013;47:9-23.
29. Alexandrova M, Bochev P, Markova V, Bechev B, Popova M, Danovska M, Simeonova V. Dynamics of free radical processes in acute ischemic stroke: influence on neurological status and outcome. J Clin Neurosci 2004;11:501-6.
30. Wang J, Huang L, Cheng C, Li G, Xie J, Shen M, Chen Q, Li W, He W, Qiu P, Wu J. Design, synthesis and biological evaluation of chalcone analogues with novel dual antioxidant mechanisms as potential anti-ischemic stroke agents. Acta Pharm Sin B 2019;9:335-50.
31. Yablonskiy DA, Bretthorst GL, Ackerman JJ. Statistical model for diffusion attenuated MR signal. Magn Reson Med 2003;50:664-9.
32. Paschoal AM, Leoni RF, Dos Santos AC, Paiva FF. Intravoxel incoherent motion MRI in neurological and cerebrovascular diseases. Neuroimage Clin 2018;20:705-14.
33. Zhou XJ, Gao Q, Abdullah O, Magin RL. Studies of anomalous diffusion in the human brain using fractional order calculus. Magn Reson Med 2010;63:562-9.
34. Poblador Rodriguez E, Moser P, Dymerska B, Robinson S, Schmitt B, van der Kouwe A, Gruber S, Trattnig S, Bogner W. A comparison of static and dynamic ΔB0 mapping methods for correction of CEST MRI in the presence of temporal B0 field variations. Magn Reson Med 2019;82:633-46.

Cite this article as: Zhou Y, Wang Z, Shaghaghi M, Zhang G, Zhu H, Wu D, Lu J, Yan S, Zhang S, Li L, Li J, Cai K, Zhu W. Proton exchange rate of chemical exchange saturation transfer MRI constructed from direct saturation-removed omega plots to improve the assessment of patients with ischemic stroke. Quant Imaging Med Surg 2022;12(10):4865-4874. doi: 10.21037/qims-22-78

Supplementary

Table S1 The x-intercept and slope in the linear fitting of the omega plots

	Acute (≤3 d), n=35	Subacute (3–14 d), n=30	Chronic (>14 d), n=31	P†
X-intercept of lesion (-10^{-6}) (95% CI)	1.17 (1.10–1.23)	1.30 (1.24–1.37)	1.36 (1.28–1.44)	0.001
X-intercept of mirror tissue (-10^{-6}) (95% CI)	1.67 (1.61–1.73)	1.73 (1.67–1.80)	1.76 (1.70–1.82)	0.09
Slope of lesion (10^5) (95% CI)	1.69 (1.61–1.78)	1.70 (1.64–1.76)	2.00 (1.84–2.15)	<0.001
Slope of mirror tissue (10^5) (95% CI)	1.43 (1.39–1.47)	1.44 (1.40–1.48)	1.41 (1.38–1.44)	0.514

†, difference among three groups; CI, confidence interval.

https://dx.doi.org/10.21037/qims-22-78